Alternating traveltime tomography and waveform inversion for near-surface imaging

Mengyao Sun, Jie Zhang, and Wei Zhang, University of Science and Technology of China*

Summary

Near-surface imaging often plays a significant role in producing quality data processing results for the deep subsurface structure in land and shallow marine environments. First-arrival traveltime tomography is a common approach for near-surface imaging due to its high efficiency and simplicity. However, the method faces with issues of missing hidden layers and resolving the structures with low resolutions. On the other hand, waveform inversion should offer better solutions for dealing with these issues but may suffer from the cycle skipping problem. We intend to use the advantages and reduce the disadvantages of the two methods by developing a new strategy of alternately applying traveltime tomography and waveform inversion through iterations. First-arrival traveltime tomography applies a wavefront raytracer and a nonlinear inversion approach. Waveform inversion is a multiscale approach in which a wavelet transform is applied in the data domain to better handle the cycle skipping problem. By alternating the two inversions rather than performing a joint inversion, we reduce the memory requirements and avoid non-physical scaling problems between the two methods. With a synthetic test and real data example, we demonstrate that alternating inversions minimize two separate objective functions at the same time and constrain the near-surface structures fairly well compared with the waveform inversion alone.

Introduction

Solving near-surface statics problem is often critical in land or shallow marine seismic data processing. First-arrival traveltime tomography (Zhang and Toköz, 1998; Zhu et al., 2008) is a standard approach for imaging the near-surface velocity structures due to its efficiency and simplicity. However, traveltime tomography may fail to reveal hidden layers and may also fail to resolve detailed structures with high resolution. Full-waveform inversion (FWI) has been developed to address these problems (Tarantola, 1988). However, the objective function of FWI includes numerous local minima. In the data domain, the problem is well known as cycle skipping if the predicted data from a starting model differs from the acquired data by more than half a period (Shin and Cha, 2009; Fei et al., 2012; Beaten et al., 2013; Chi et al., 2014). For getting over the cycle skipping problem, many methods have been developed, such as multiscale waveform inversion method (Bunks et al., 1995), which gradually inverts from low-wavenumber to high-wavenumber structures. The precondition of the multiscale method is that the global solution on one scale is always in the convex neighborhood of the global minimum of the next smaller scale. However, it cannot be theoretically guaranteed valid for all applications. The joint inversion method is considered another way to solve the local minima problem (Zhang et al., 2014). The challenges of performing joint inversion include the selection of a non-physical scaling factor between different inversion-problems, which is very essential to the final result.

In this study, we present a different strategy for fitting both traveltime and waveform data for near-surface imaging. As a result, we alternately solve one traveltime tomography problem and one waveform inversion problem during each iteration. Because the approach alternately executes inversions, it saves memory required for the joint inversion and avoids a non-physical scaling factor between different inversion-problems. We apply this new method to one synthetic example and a field dataset, the results are encouraging.

Theory

The alternating inversion is performed by applying waveform inversion and traveltime tomography alternately. The first-arrival traveltime tomography applies a wavefront raytracer and a nonlinear inversion approach. Waveform inversion is a multiscale approach in which the wavelet transform is applied in data domain to better handle the cycle skipping problem.

At the beginning of the inversion, the initial model of the alternating inversion is built by the first-arrival traveltime tomography. The multiscale waveform inversion is first performed on the large-scale data that we select. The result obtained by the waveform inversion is the initial model and the structural constraint of the traveltime tomography. The procedures should be then repeated in the next iteration and for the next smaller scale. The workflow of the alternating inversion is shown as follows:

do $scale = scale_{start}, scale_{end}$
  do $iter = 1, itermax$
    $\boldsymbol{m}_{ini} = \boldsymbol{m}_{tt}$
    $\Phi_{scale}(\boldsymbol{m}_{fwi}) = \sum_{s,r} \int (s_{scale}(\boldsymbol{x}_r, \boldsymbol{x}_s, t; \boldsymbol{m}_{fwi}) - \mathrm{d}_{scale}(\boldsymbol{x}_r, \boldsymbol{x}_s, t))^2 dt + \alpha \left\| \boldsymbol{L}(\boldsymbol{m}_{fwi}) \right\|^2$
    $\boldsymbol{m}_{ini} = \boldsymbol{m}_{fwi}$
    $\Psi(\boldsymbol{m}_{tt}) = \|\boldsymbol{d}_{obs} - G(\boldsymbol{m}_{tt})\|^2 + \lambda \|\boldsymbol{L}(\boldsymbol{m}_{tt} - \boldsymbol{m}_{ini})\|^2$
  enddo
enddo

Here, $scale$ is the current scale for the inversion. $iter$ is the current iteration of the inversion, $itermax$ is the maximum

iteration number we set, $scale_{start}$ and $scale_{end}$ are the start scale and the final scale, respectively. $\boldsymbol{m}_{ini}$ is the initial model for the current inversion method. $\boldsymbol{m}_{fwi}$ is the inversion result of the multiscale waveform inversion at this stage, $\boldsymbol{m}_{tt}$ is the first-arrival traveltime tomography result at this stage. $s(\boldsymbol{x}_r, \boldsymbol{x}_s, t; \boldsymbol{m})$ represents the synthetic waveforms, $d(\boldsymbol{x}_r, \boldsymbol{x}_s, t)$ is the observed waveforms. $\boldsymbol{x}_r$ and $\boldsymbol{x}_s$ are the positions of the receivers and shots, respectively. $\boldsymbol{m}$ is the model slowness and t is the time window for the inversion. $\boldsymbol{L}$ is the Laplacian operator for model regularization and α is a constant parameter for balancing the data misfit and the model regularization. $\boldsymbol{d}_{obs}$ is the observed traveltime data and $G(\boldsymbol{m})$ contains the calculated traveltimes. λ has the same meaning as α. Finally, the output is $\boldsymbol{m}_{tt}$ or $\boldsymbol{m}_{fwi}$, because they are almost the same in the end of the entire inversion procedure.

Synthetic test

We conduct the alternating inversion with a synthetic test. In the following we will use the result obtained by the waveform inversion method alone as the comparison to evaluate the improvements of the alternating method. Figure 1a shows the true model of the synthetic test. The model includes two layers imbedded in a background with a constant gradient and it measures 5000 m × 600 m and the grid size is 10 m × 10 m. The sketch of the acquisition geometry is also shown in Figure 1a. We use red and yellow dots to represent the shots and receivers, respectively. The survey geometry includes 80 shots and 160 receivers for every shot with a 60 m shot spacing and 30 m receiver spacing, respectively. The true traveltime data are calculated by a wavefront raytracing technique. The seismograms of this model are generated by an acoustic Finite Difference (FD) method (Zhang and Zhang, 2011) with a Ricker wavelet as the source wavelet. The same method is used for the subsequent waveform inversion. After obtaining the simulated true data, we decompose the waveforms into eight levels and reconstruct them from scale 5 down to scale 4 and scale 0 which formally captures all original signals.

Figure 1b shows the initial model for the two different inversion methods and it is built by first-arrival traveltime tomography. First, we perform the wavelet-based multiscale waveform inversion without the traveltime information being involved. The inversion results of different scales are displayed in Figure 1c, e, and g. Figure 1g is the final result. We then perform the alternating inversion employing the same initial model. Figure 1d, f, and h display the inversion results obtained by the alternating inversion method, and Figure 1h is the final result. In the results obtained by the two different methods, we observe that when the data scale turns form large to small, the structures are inverted gradually and the resolution becomes higher. For the waveform inversion method alone, we notice that although it can roughly invert the two layers, the shapes are distorted, and some artifacts are present in the results, especially in the shallow part. That is because the cycle skipping occurs and leads a poor traveltime fitting which is essential for the shallow velocity structure imaging. However, the result obtained by the alternating inversion reveals the two layers with the better positions, better velocity values, and better structure shapes.

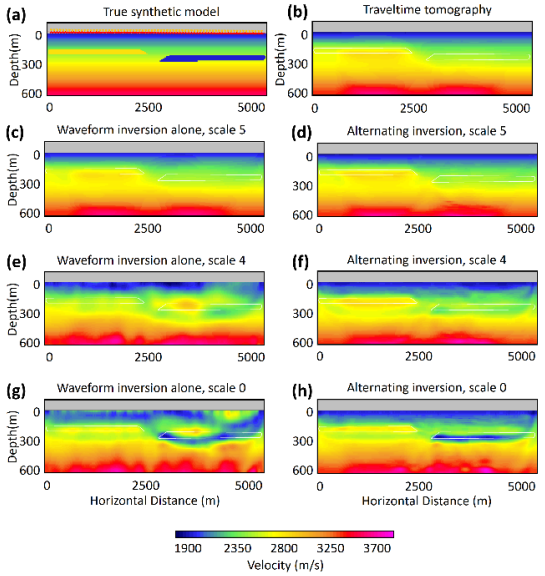

Figure 1: A synthetic test and comparison. The inversion result obtained by the two different methods. The white lines mark the true positions of the layers. (a) The true model. (b) The initial model. (c), (e), and (g) are the results of scale 5, scale 4, and scale 0, which are obtained by performing the waveform inversion method alone. (d), (f), and (h) are the results of applying the alternate inversion method associated with scale 5, scale 4, and scale 0 data representations.

We show the quality control of waveform fitting and traveltime fitting of this synthetic test in Figure 2. Figure 2a and b display the waveform and traveltime overlay of the two methods. The black waveforms are the simulated true seismograms and the red waveforms are the synthetics of the final inversion results. The green dots represent the simulated true traveltimes and the blue ones represent the traveltimes of the final inversion results. Both waveforms and traveltimes show better fitting performance for the alternating inversion method compared with the waveform inversion method alone. Furthermore, a notable cycle skipping phenomenon occurs in Figure 2a. However, it converges to the global minimum for the alternating inversion method by involving both waveform and traveltime information and avoids dropping into the local minima. The waveform and traveltime misfit curves of the waveform inversion method alone are shown in Figure 2c

and e, the corresponding curves of alternating inversion are shown in Figure 2d and f. The reciprocal error of the first-arrival picks in this synthetic test is approximately 5 ms. Both the waveform and traveltime misfit present large differences for the two methods. We observe that, for the waveform inversion method alone, the traveltime misfit increases with the number of iterations while the waveform misfit actually decreases. That should be an evidence of cycle skipping. That means, with the waveform inversion moving on, the waveforms fit the wrong ones, which also decreases the waveform misfit but the traveltime misfit should be increased. This indicates that the waveform inversion method alone may drop into a local minimum. This conclusion is consistent with the comparison of the data overlay as well.

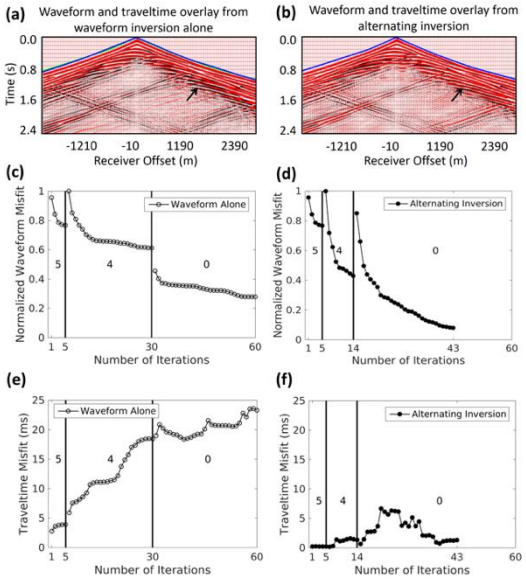

Figure 2: The quality control of waveform fitting and traveltime fitting for the synthetic test. The black waveforms are the simulated true data. The red waveforms are the synthetics of the final inversion results. The green dots are the simulated true traveltimes and the blue ones are the synthetics of the final inversion results. (a) The overlay of the waveform inversion method alone. The black arrows point out the waveforms where the cycle skipping occurs. (b) The overlay of the alternating inversion method. (c), (d), (e), and (f) are the misfit curves of the synthetic test. (c) and (d) are the normalized waveform misfit of the waveform inversion method alone and the alternating inversion method, respectively. (e) and (f) are the traveltime misfit of the two methods, respectively.

Real data application

A 2-D land dataset acquired from the Yumen Oil Field in Northwest China, is employed to test the performance of the alternating inversion in a real case. This area is well known for its complex geology and difficulties in imaging the subsurface with seismic methods. In September 2004, PetroChina conducted a multichannel large-offset 2-D survey in this area to image the complex imbricate structure, which is associated with the Yumen reservoir beneath the high-velocity Kulong Shan allochthonous rocks. The near-surface correction is the first challenging problem for data processing. The topography of this area presents large variations: the elevation alone the survey line varies between 3500 m and 2000 m from south to north. To capture the deep wide-angle reflections and refractions, the acquisition geometry followed a common spread configuration. The total number of shots (dynamic sources) in this survey line is 211, with a shot spacing of 200 m, and the shot hole depth varies from 20 to 30 m. We select 137 shots from the dataset to implement this field data in our inversion method. Therefore, the survey line in this case is about 28 km. The maximum number of receivers in one shot is 151 for a maximum offset of approximately 1500 m.

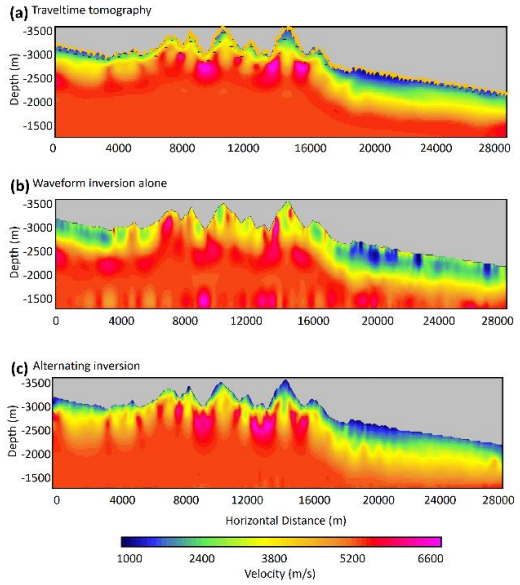

Figure 3: The real data application. (a) The initial model built by the first-arrival traveltime tomography. (b) The final result of the waveform inversion method alone. (c) The final result of the alternating inversion method.

We first manually pick the first arrivals and build the initial model of the near surface by first-arrival traveltime tomography (Figure 3a). The initial model shows strong lateral and vertical velocity variations below the rugged topography. Such a complex near-surface structure encourages us to further improve the imaging quality by involving the waveform inversion. We then implement a series of data preprocessing procedures, such as band-pass filtering, trace editing, muting the data and saving the early

arrival part of approximately 200-300 ms. Then we decompose the preprocessed data into ten scales and start the two inversion methods from scale 6 down to scale 5, scale 4, and scale 0. Figure 3b shows the final result obtained by the waveform inversion method alone. Additionally, we show the result obtained by the alternating inversion in Figure 3c.

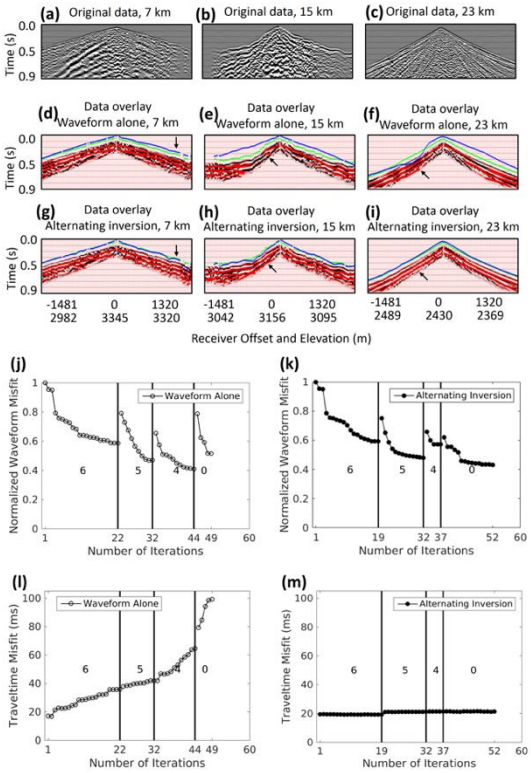

Figure 4: The quality control of the waveform fitting and traveltime fitting for the real data application. (a), (b), and (c) are the original shot gathers which are located at horizontal distance of 7 km, 15 km, and 23 km, respectively. (d), (e), and (f) are the overlay of the waveform inversion method alone for these three shots. (g), (h), and (i) are the overlay of the alternating inversion method for the three shots. (j), (k), (l), and (m) are the misfit curves of the real data application. (j) and (k) are the normalized waveform misfit the the waveform inversion method alone and the alternating inversion method, respectively. (l) and (m) are the traveltime misfit of the two methods, respectively.

The two solutions obtained by the different methods present very different structures for this area. To validate the inversion results, we display the quality control of waveform fitting and traveltime fitting of three shot gathers located at different positions (Figure 4). The horizontal location of the tree shots are 7 km, 15 km, and 23 km. The elevations are 3309 m, 3214 m, and 2433 m, respectively. Figure 4a, b, and c are the original data of the three shots, Figure 4d, e, and f are the waveform and traveltime overlay of the waveform inversion method alone for the three shots and the corresponding overlay displays of the alternating inversion method are shown in Figure 4g, h, and i. We observe that although the waveform and traveltime fitting of the alternating inversion solution are not perfect, they are much better compared with the result obtained by the waveform inversion method alone. This suggests that the alternating inversion method helps to fit the data better and indicates that a more reliable result can be obtained by the alternating inversion method. We also observe that notable cycle skipping occurs in the results obtained by the waveform inversion method alone and it leads to poor performance of the traveltime fitting. Consequently, many artifacts are present in the final inversion result. We also show the waveform and traveltime misfit curves of this field in Figure 4. The result is similar to the synthetic test. The waveform misfit of these two methods decreases to the same level, while the traveltime misfit presents a large difference. The reciprocal error of traveltime picks in this case is approximately 30 ms. However, the traveltime misfit of the waveform inversion method alone increases gradually with the inversion procedure and it is larger than the reciprocal error in the end.

Conclusions

We propose a new alternating inversion method by combining both wavelet-based multiscale waveform and traveltime inversions through iterations. The synthetic test verifies that this method can reduce the chance of dropping into the local minima. Compared with the wavelet-based multiscale waveform inversion alone, the alternating inversion method can maintain both the traveltime and waveform fitting at the same time. A real data application is implemented by the alternating inversion method. The better data fitting, including traveltimes and waveforms, indicates that more reasonable modeling results are revealed by the alternating inversion method. We also observe that this method can suppress the cycle skipping phenomenon to some degree in practical applications.

Acknowledgements

We gratefully acknowledge the financial support of the National Natural Science Foundation of China (Grant No. 41374132 and Grant No. 41674120). We also appreciate GeoTomo for providing TomoPlus software package with this work.

References

Baeten, G., J. W. de Maag, R. E. Plessix, R. Klaassen, T. Qureshi, M. Kleemeyer, F. ten Kroode, and R. Zhang, 2013, The use of the low frequencies in a full waveform inversion and impedance inversion land seismic case study: Geophysical Prospecting, **61**, no. 4, 701-711.

Bunks, C., Saleck F. M., Zaleski S., Chavent G., 1995, Multiscale seismic waveform inversion: Geophysics, **60**, no. 5, 1457-1473.

Chi, B., L. Dong and Y. Liu, 2014, Full waveform inversion method using envelope objective function without low frequency data: Journal of Applied Geophysics, **109**, 36-46.

Fei, T. W., Y. Luo, F. Qin, and P. G. Kelamis, 2012, Full waveform inversion without low frequencies: A synthetic study: 82nd Annual International Meeting, SEG, Expanded Abstracts, 1-5.

Shin, C., and Y. H. Cha, 2009, Waveform inversion in the Laplace-Fourier domain: Geophysical Journal International, **177**, 1067-1079.

Tarantola, A., 1988, Theoretical background for the inversion of seismic waveforms, including elasticity and attenuation: Pure and Applied Geophysics, **128**, no. 1-2, 365-399.

Zhang, J., and J. Chen, 2014, Joint seismic traveltime and waveform inversion for near surface imaging: 84th Annual International Meeting, SEG, Expanded Abstracts, 934-937.

Zhang, W. and J. Zhang, 2011. Full waveform tomography with consideration for large topography variations: 81st Annual International Meeting, SEG, Expanded Abstracts, 2539-2542.

Zhang, J. and M. N. Toksöz, 1998, Nonlinear refraction traveltime tomography: Geophysics, **63**, no. 5, 1726-1737.

Zhu, X., P. Valasek, B. Roy, S. Shaw, J. Howell, S. Whitney, N.D. Whitmore, P. Anno, 2008, Recent applications of turning-ray tomography: Geophysics, **73**, no. 5, 243-254.